

2D Bravais Lattices

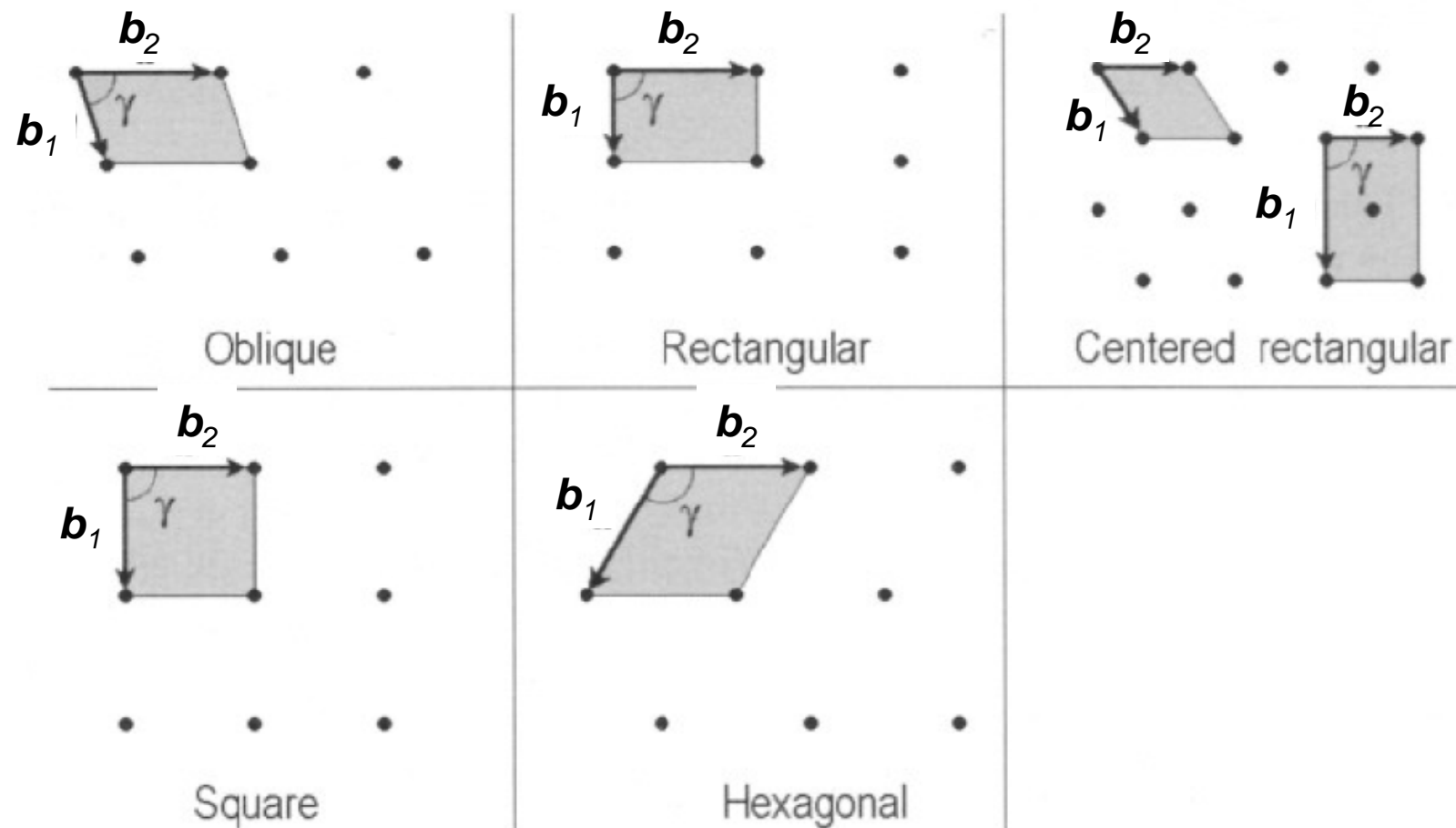


Fig.1.1

Relaxation and Reconstruction

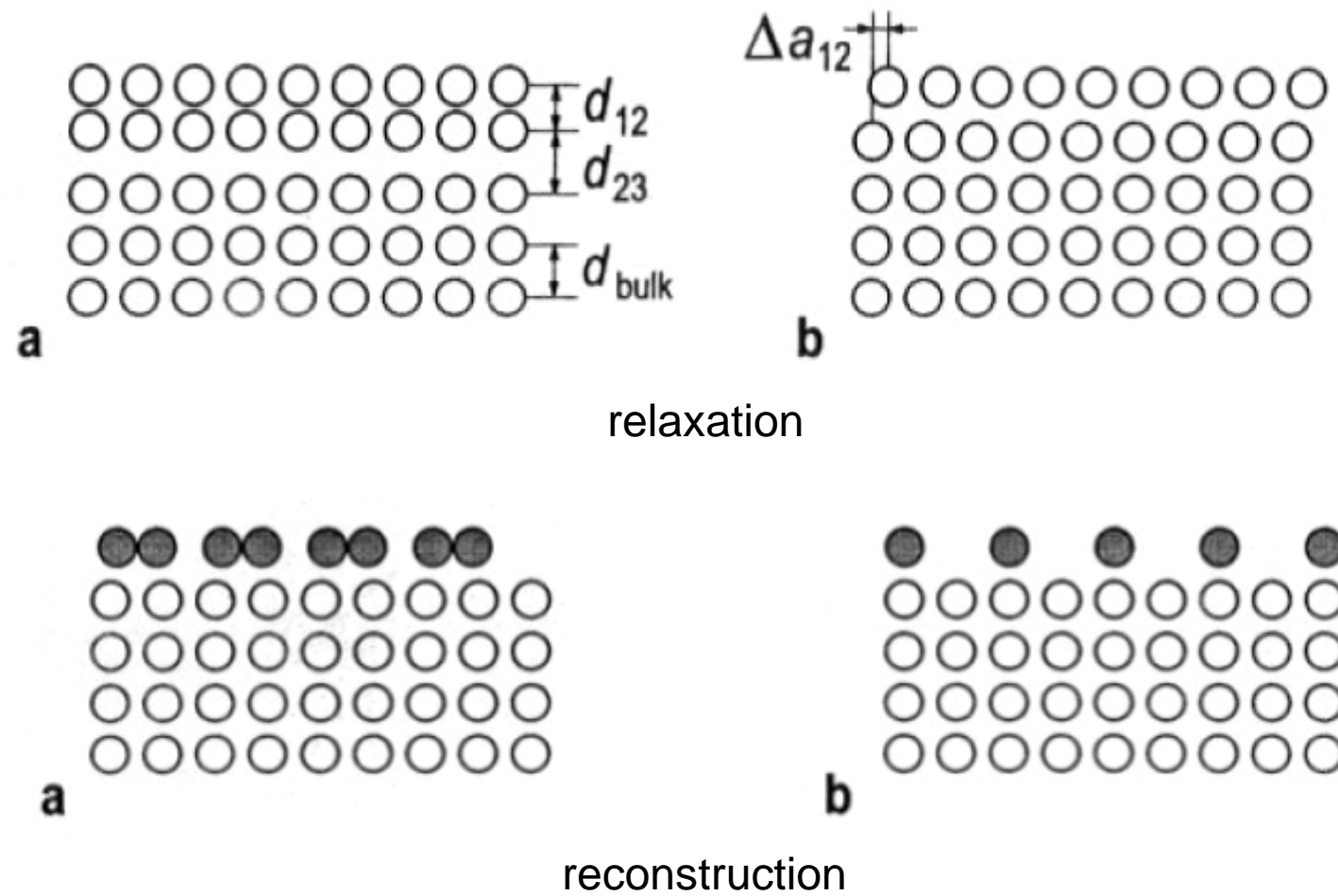


Fig.1.2

Examples for Wood's Notation and the Matrix Notation

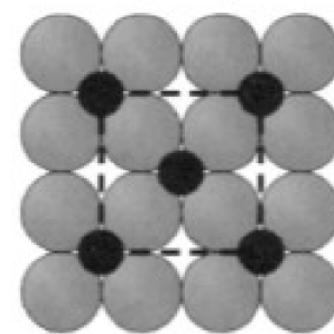
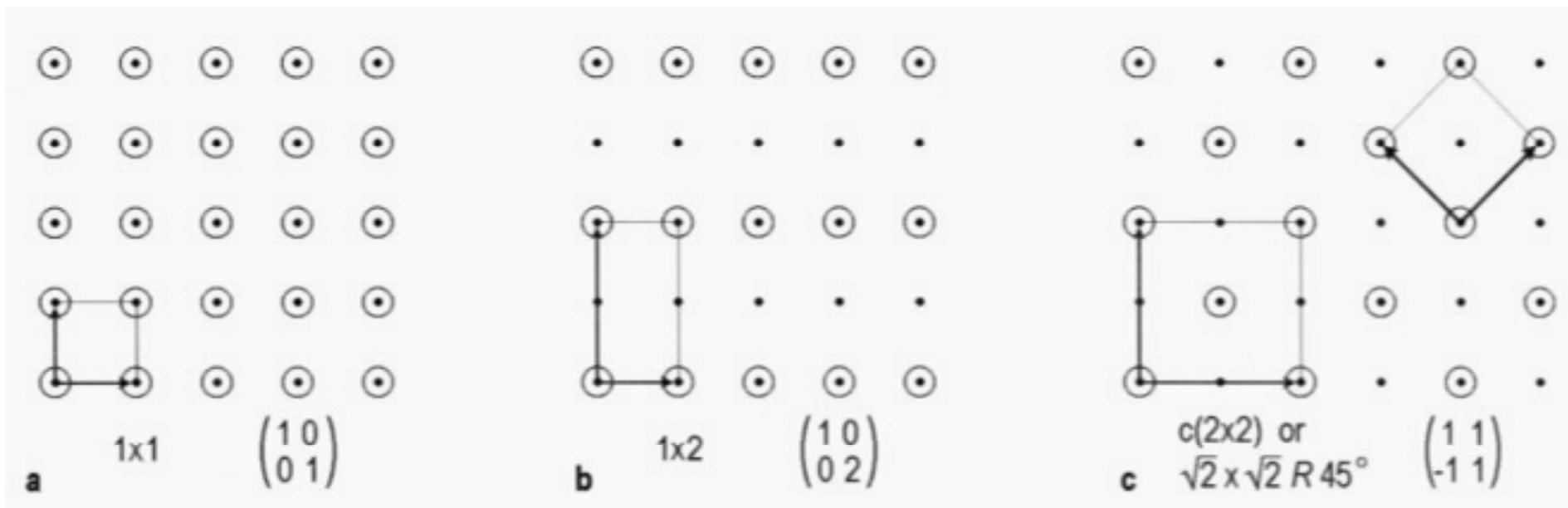


Fig. 1.3a

Examples for Wood's Notation and the Matrix Notation

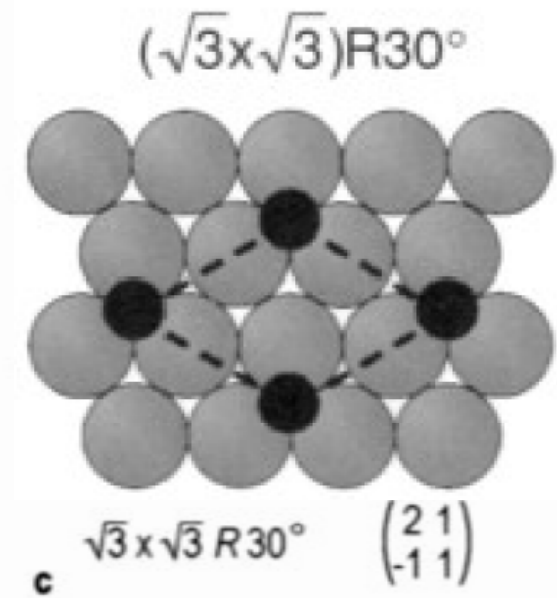
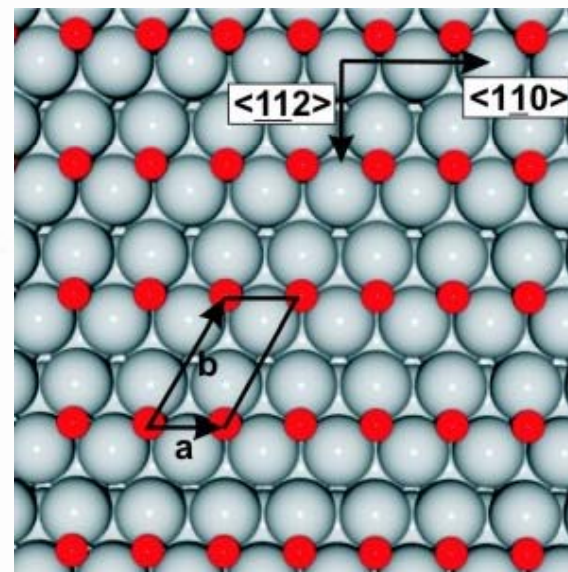
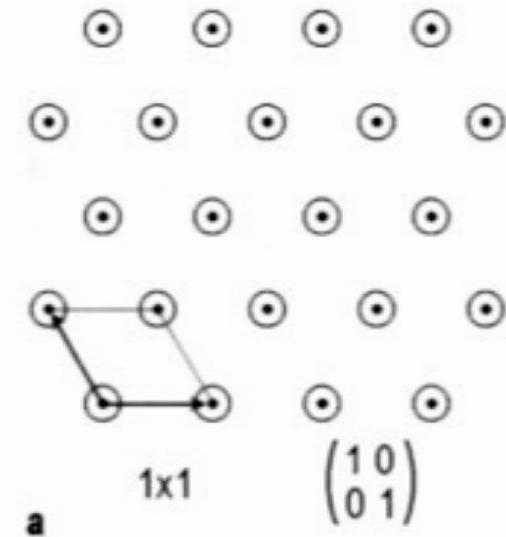


Fig.1.3b

2D Real Space and Reciprocal Space Unit Meshes and Primitive Translations

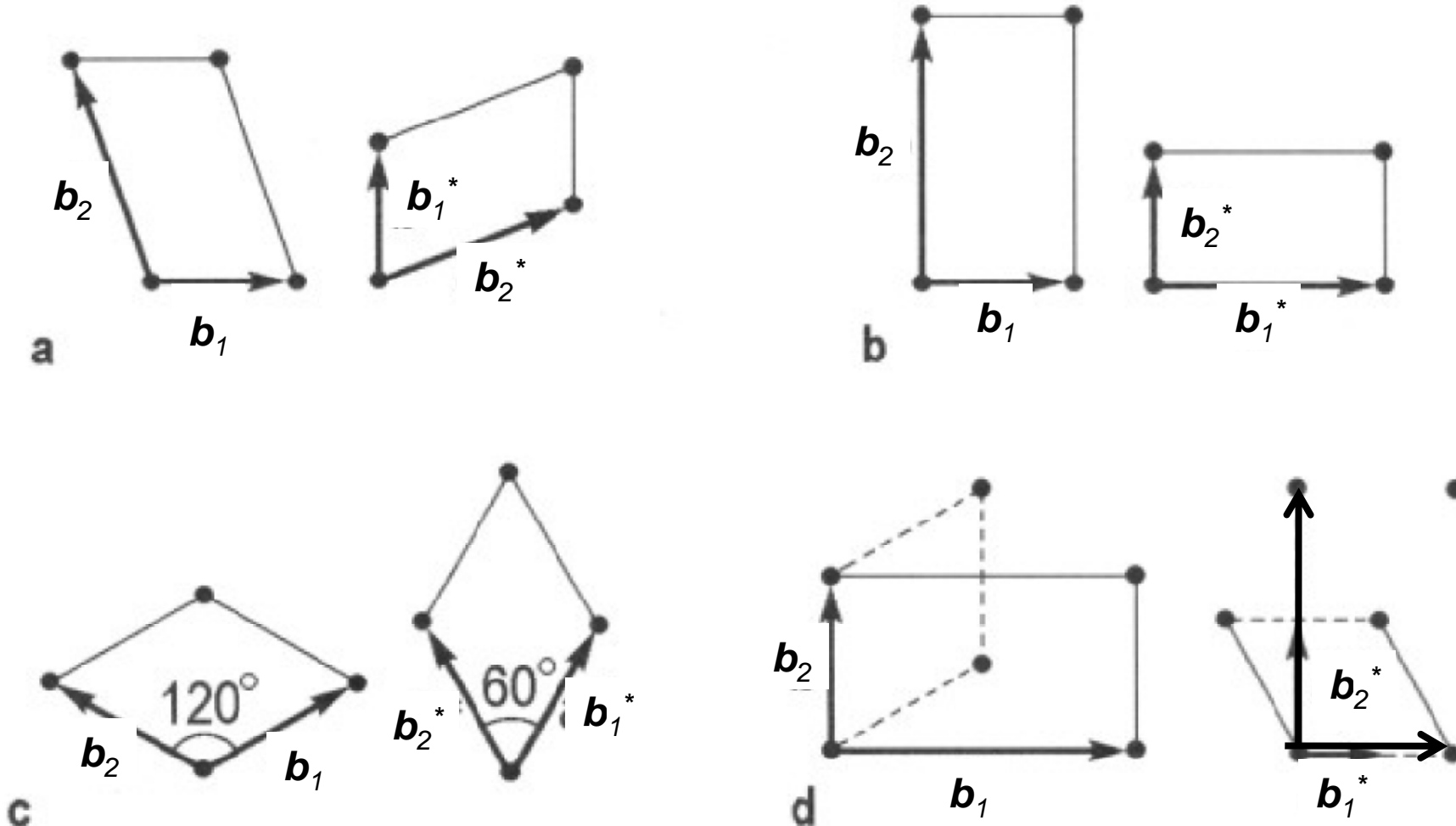


Fig.1.4

Relation Between 2D and 3D Brillouin Zones

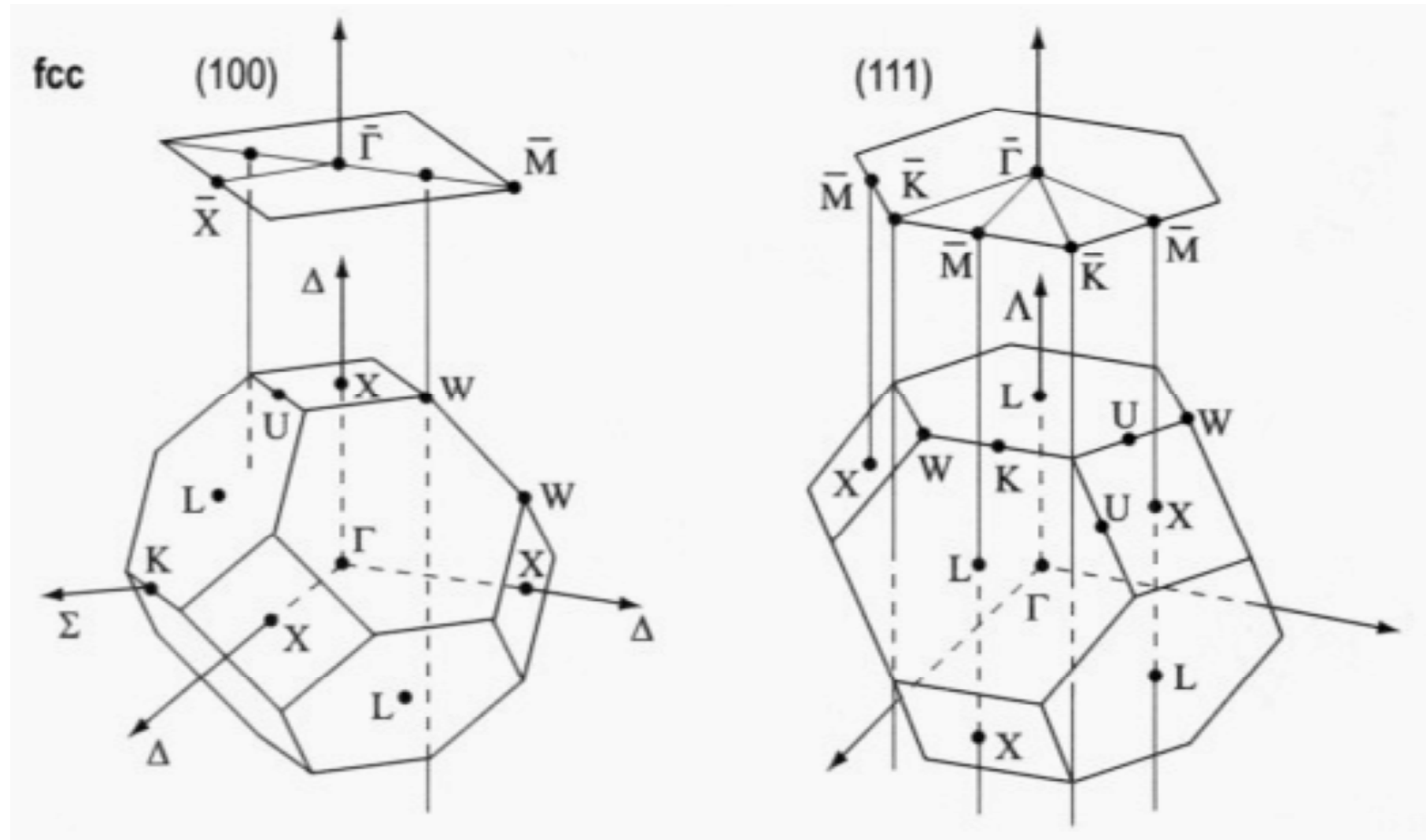


Fig.1.5

Structures of Unreconstructed Low Index fcc Surfaces

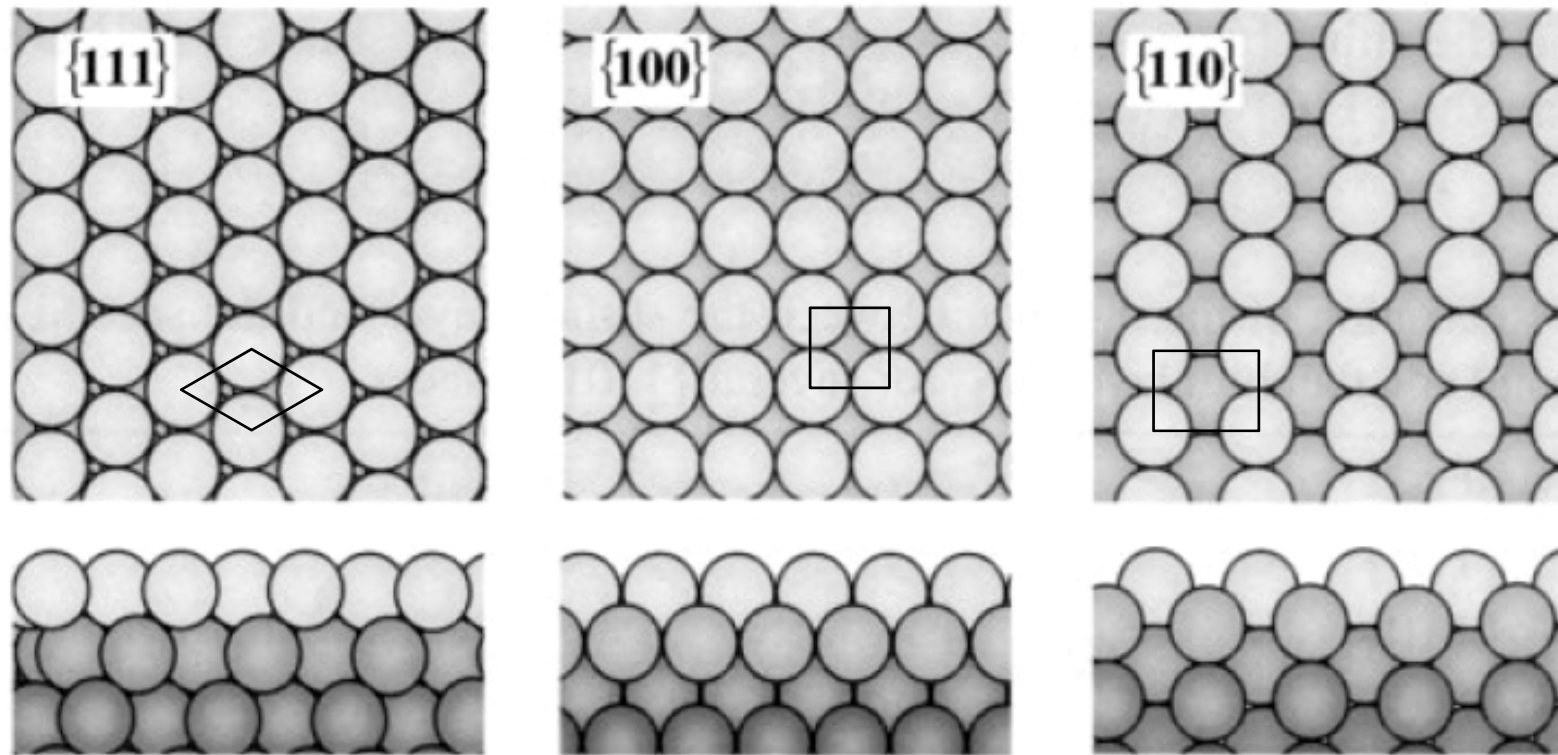


Fig. 1.6

Dependence of Bond Strength on Coordination

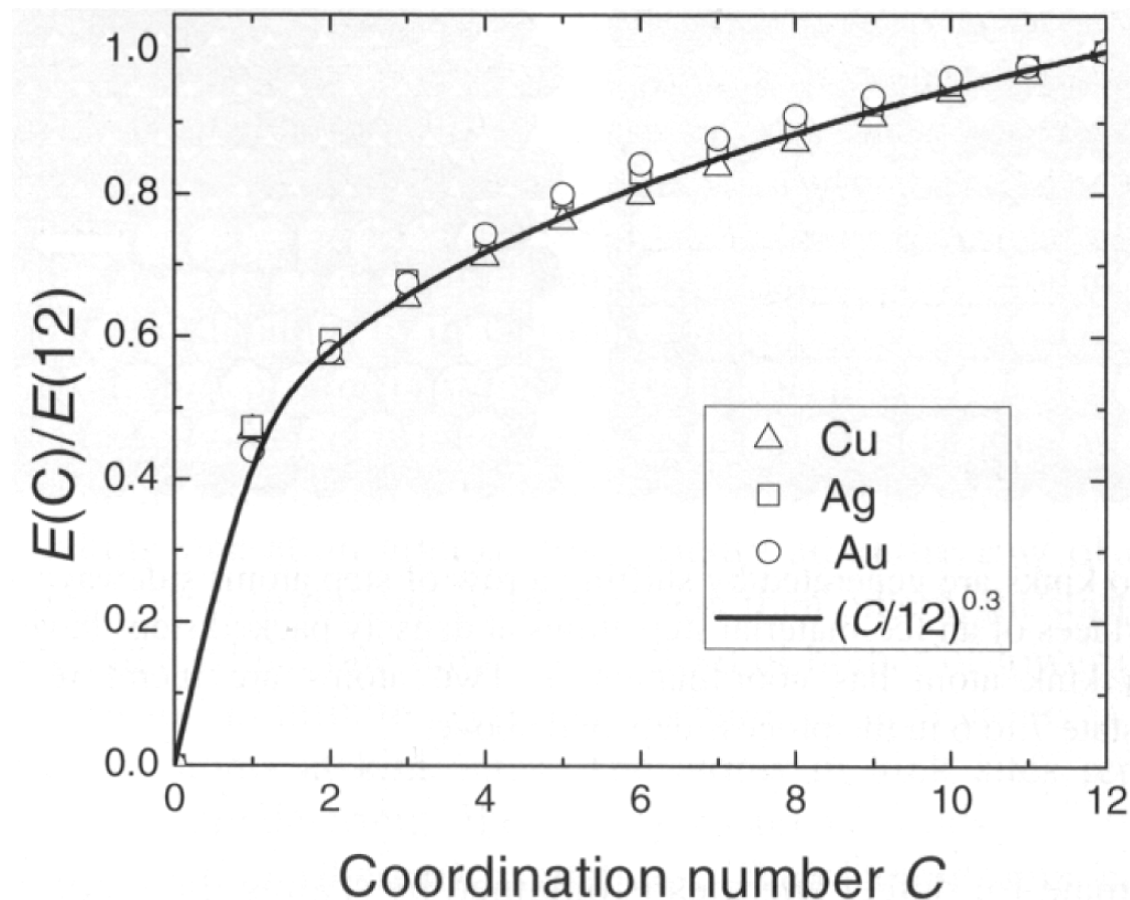


Fig. 1.7

Relaxation of Unreconstructed fcc(110) Surfaces

Table 1.2. Relaxation of the distance between the surface layer and the second layer Δd_{12} and the second and the third layer Δd_{23} for several {110} surfaces.

Material	Δd_{12}	Δd_{23}
Cu{110}	-9%	+3%
Ag{110}	-8%	0%
Ni{110}	-9%	+3.5%
Pd{110}	-5%	+1%
Rh{110}	-7%	+2%

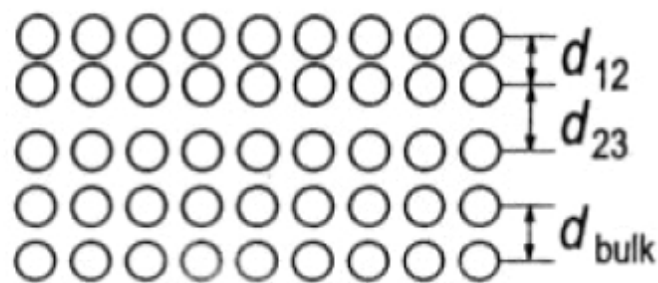


Fig. 1.8

Quasi-Hexagonal Reconstruction of Pt(001) 5xn ($n \approx 30$)

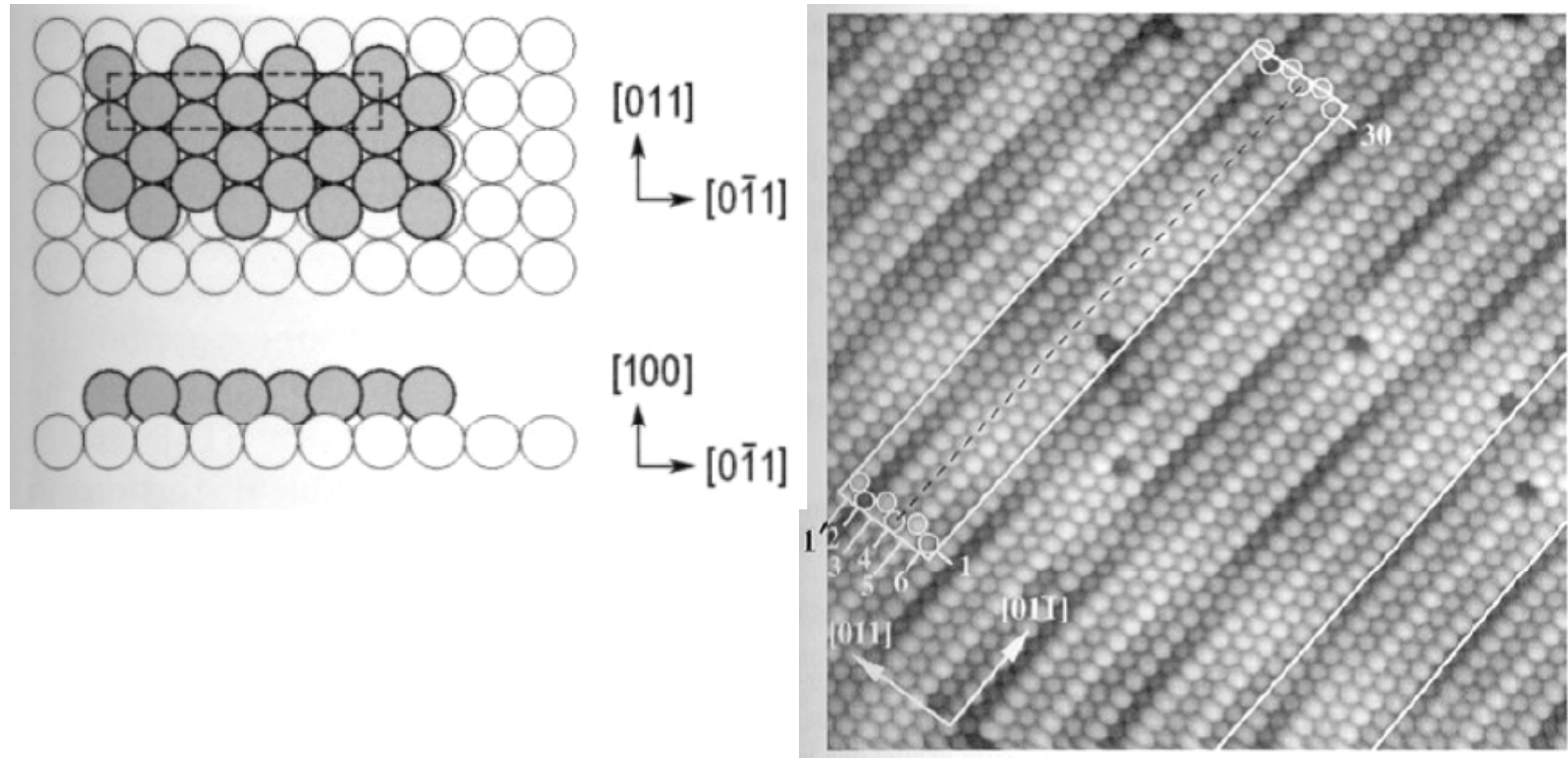
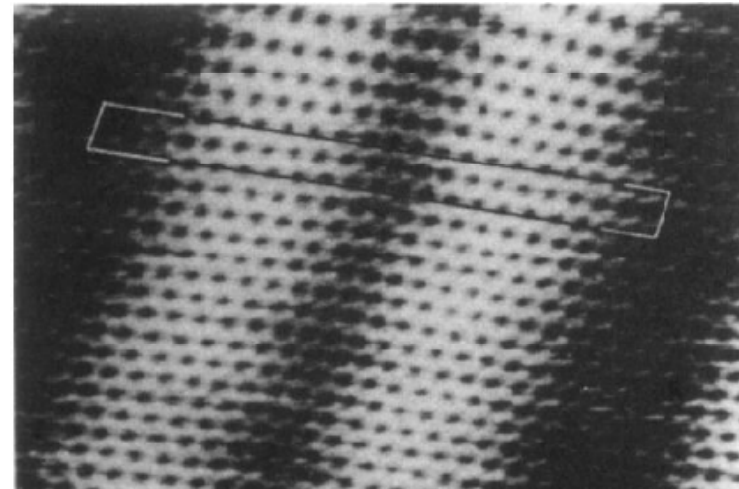


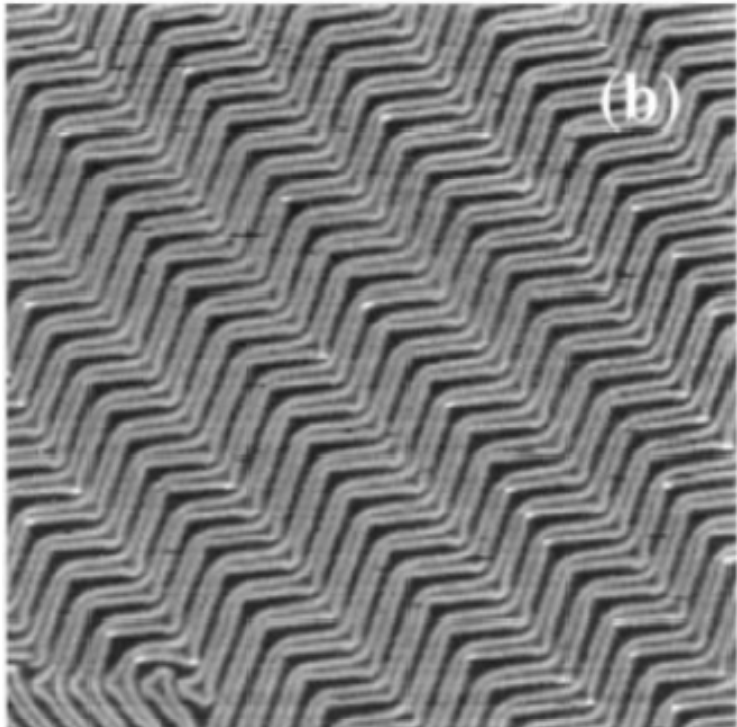
Fig. 1.9

Herringbone Reconstruction of Au(111)
(Double Soliton Reconstruction)



fcc-sites

hcp-sites



fcc-sites

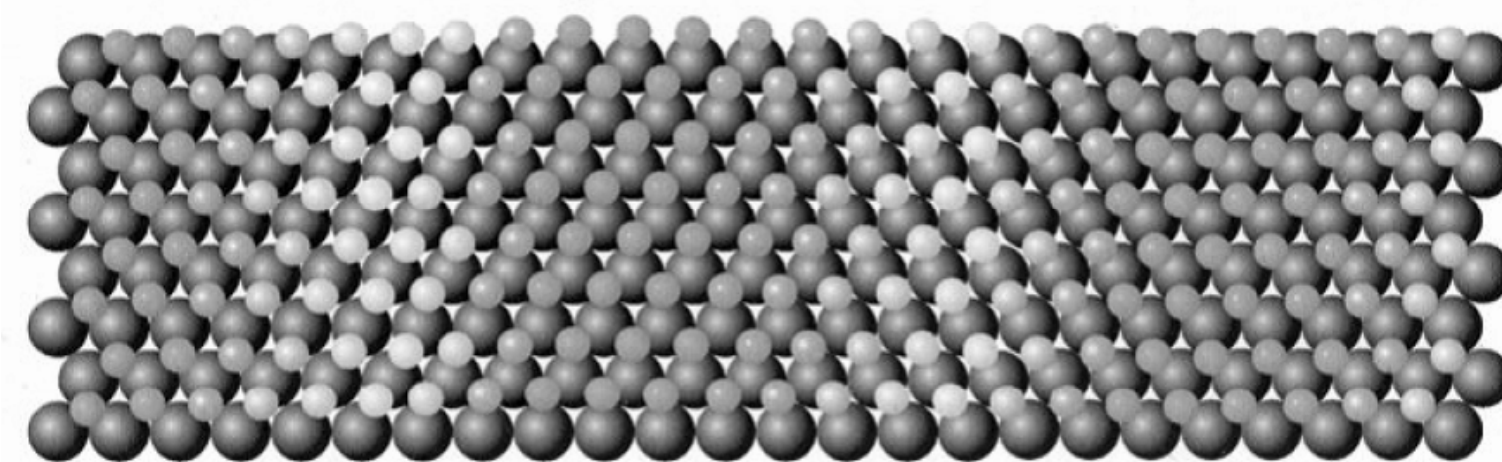
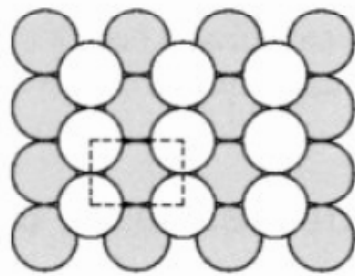


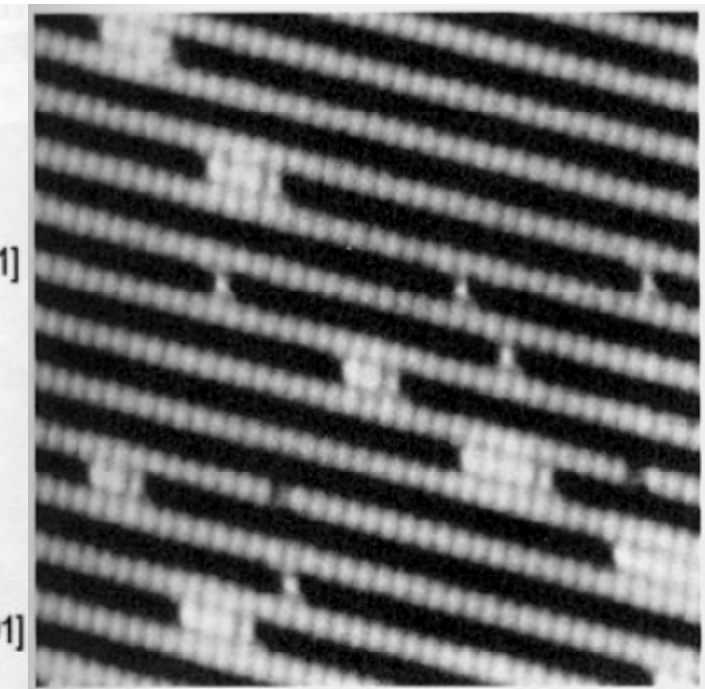
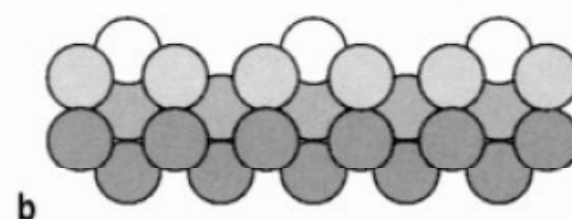
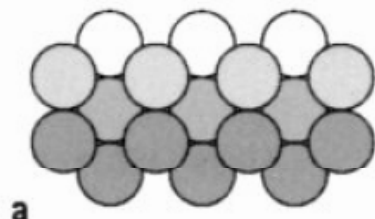
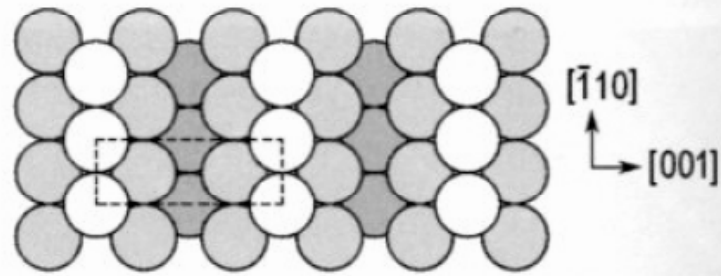
Fig. 1.10

Missing Row Reconstruction of Pt(110)

Pt(110)1x1 ideal termination



Pt(110)1x2 missing-row reconstruction



STM topograph of Pt(110) with
small amount of Pt deposited

Fig. 1.11

Structures of Unreconstructed Low Index bcc Surfaces

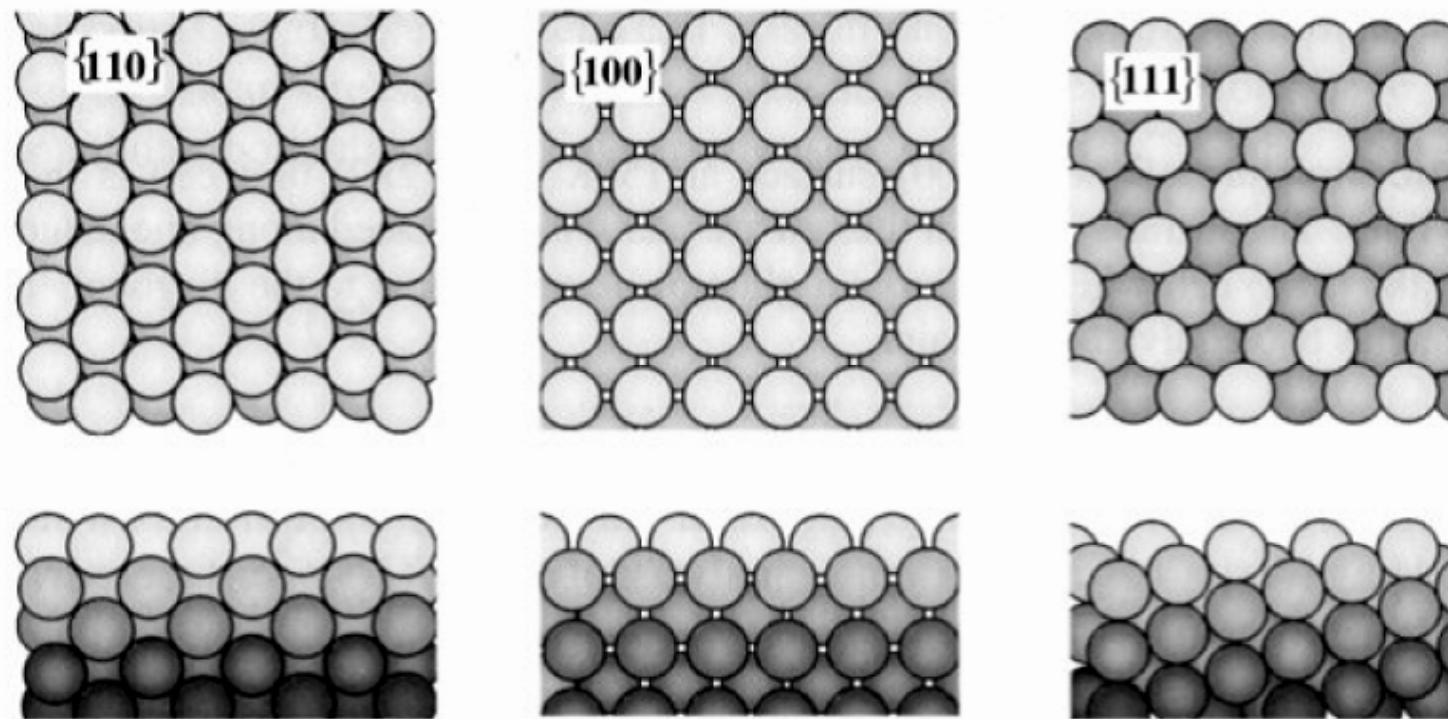


Fig. 1.12

W(110) 2x2 Reconstruction

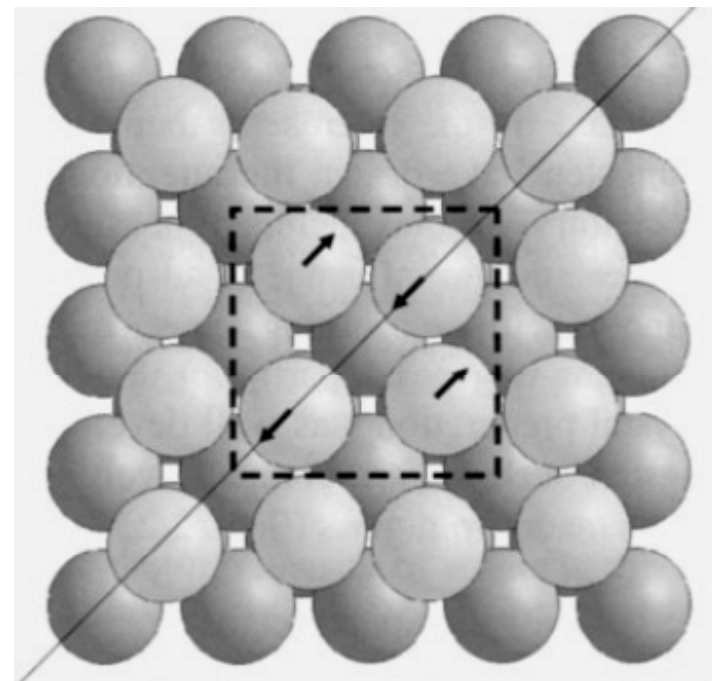
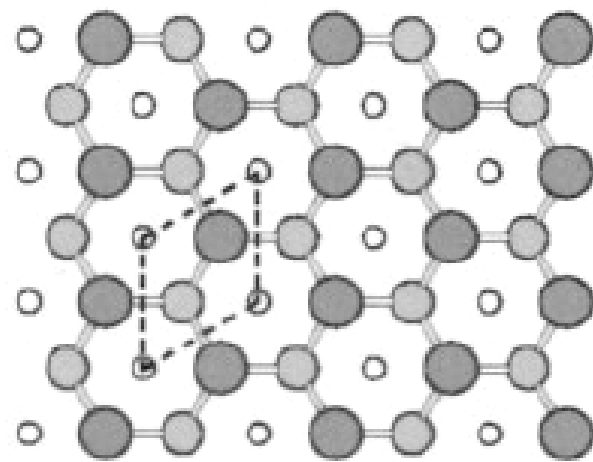


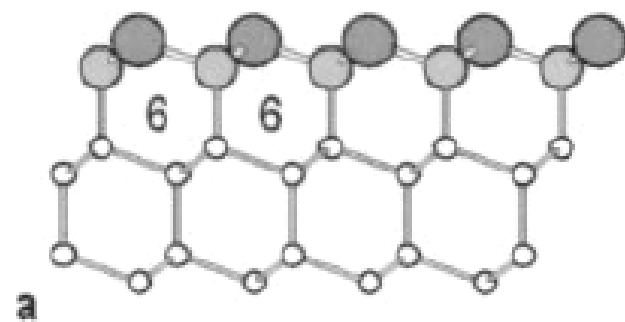
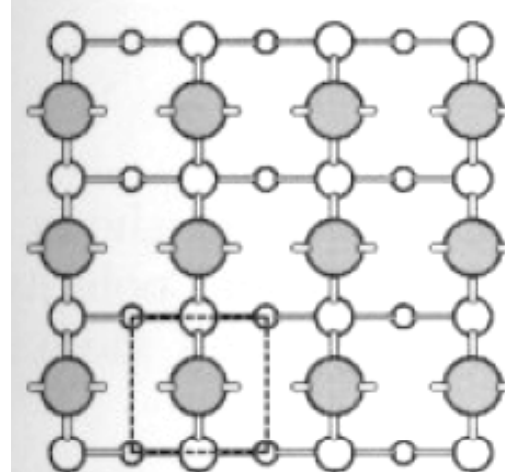
Fig. 1.13

Unreconstructed Surfaces of the Diamond Structure

(111)



(100)



dashed lines: surface unit cells

Fig. 1.14

Si(111) 7x7 Reconstruction: DAS or Dimer Adatom Stacking Fault Model

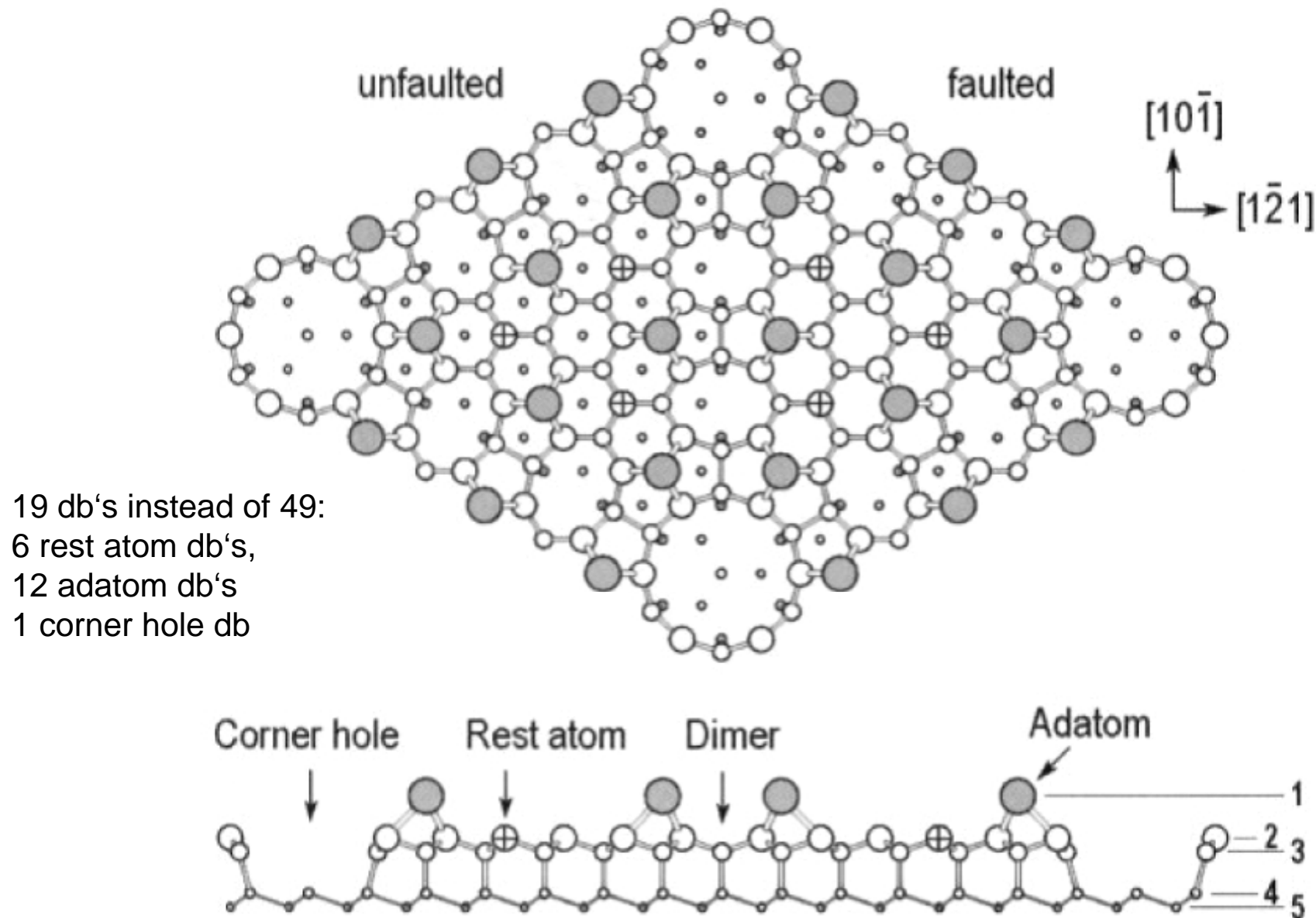


Fig. 1.15

Si(111) 7x7 Reconstruction: DAS or Dimer Adatom Stacking Fault Model

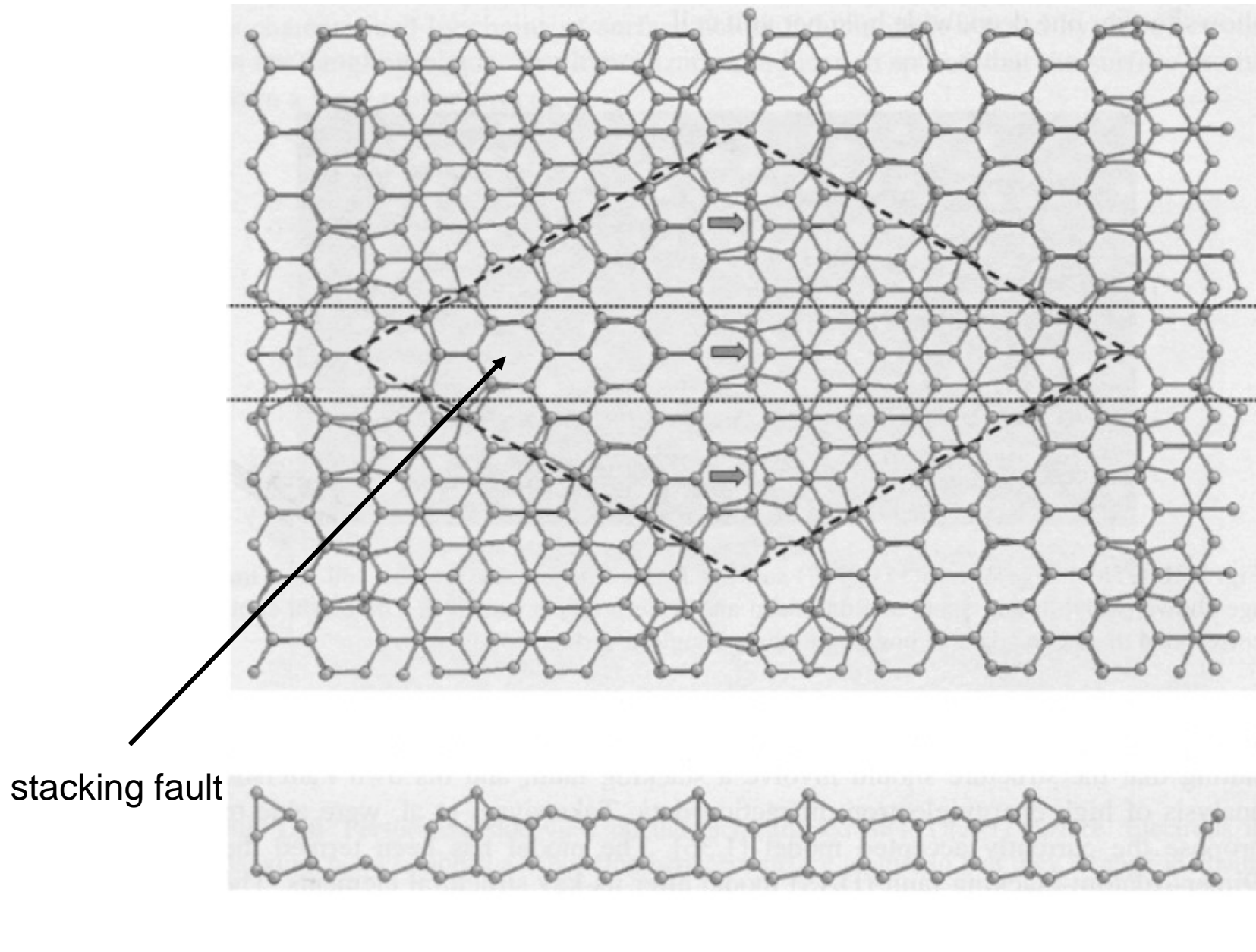
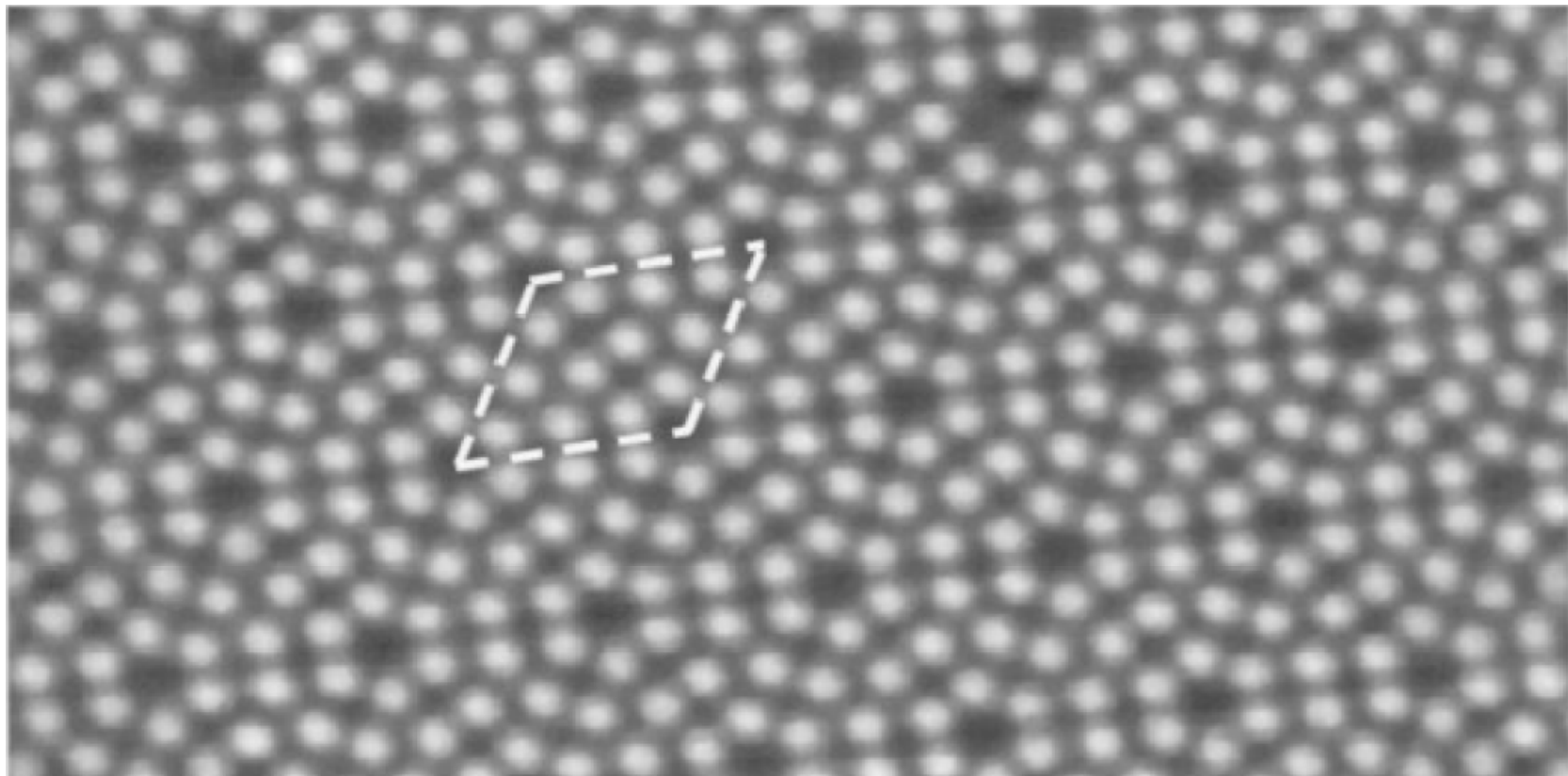


Fig. 1.16

Si(111) 7x7 Reconstruction: STM image of unoccupied states



positive sample bias,
unoccupied states
adatoms visible

Fig. 1.17

Si(100) 2x1 Dimer Reconstruction

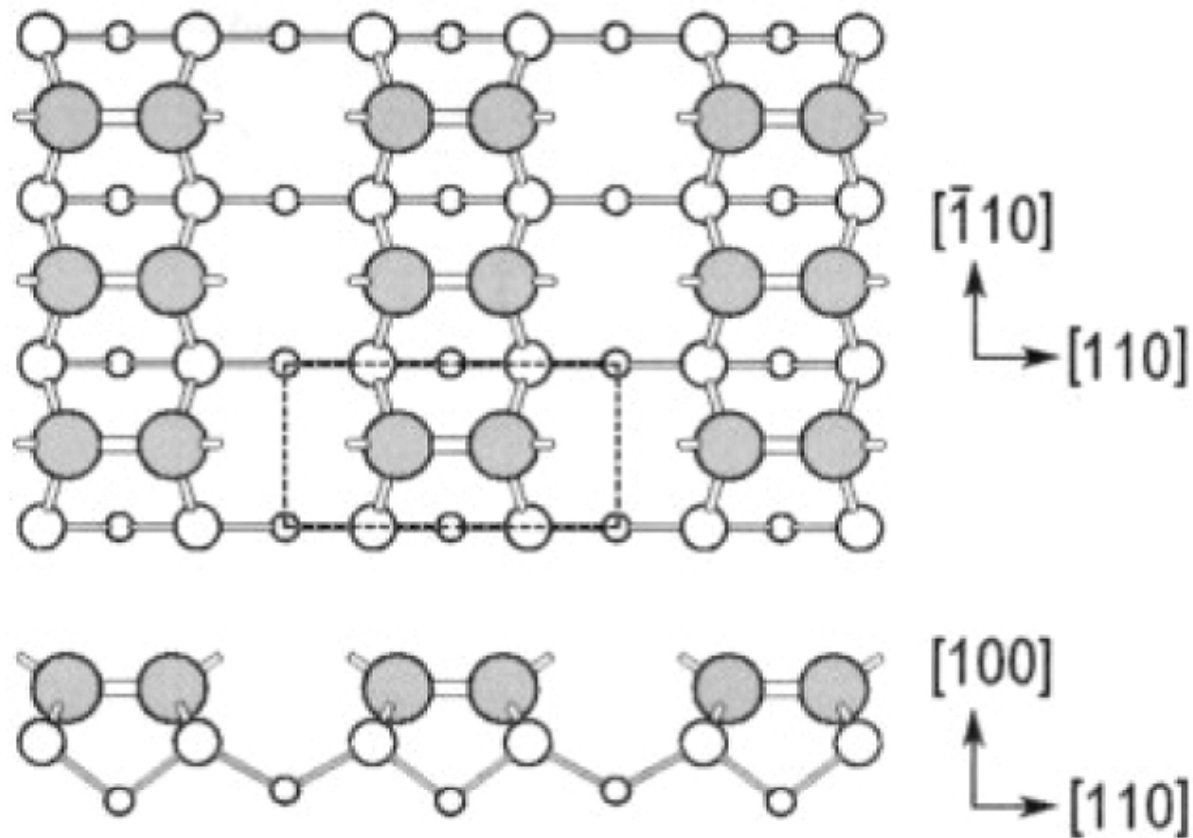
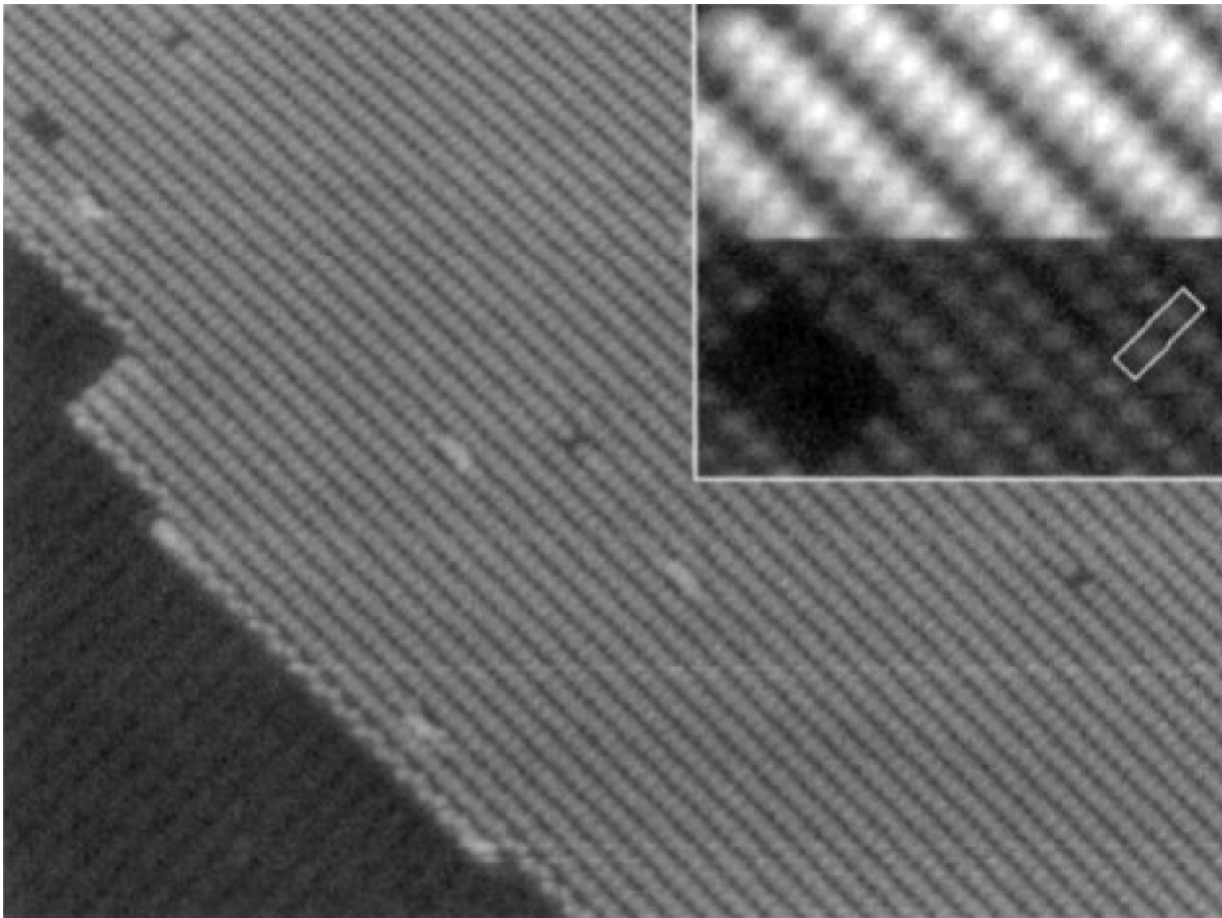


Fig. 1.18

Si(100) 2x1 Dimer Reconstruction: STM Topograph



occupied states
(negative sample bias)

unoccupied states
(positive sample bias)

Fig. 1.19

Si(001) c(4x2) Buckled Dimer Reconstruction

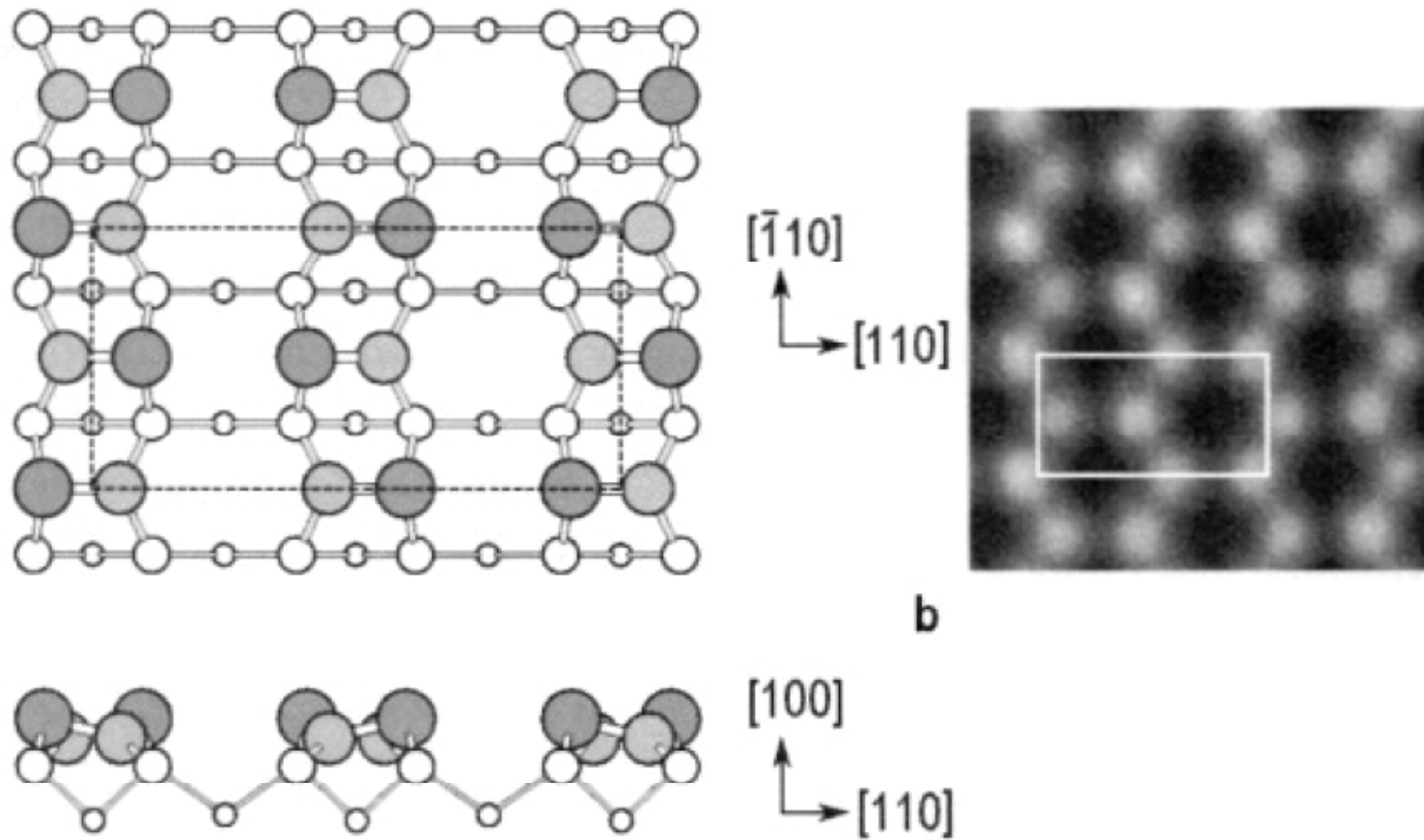
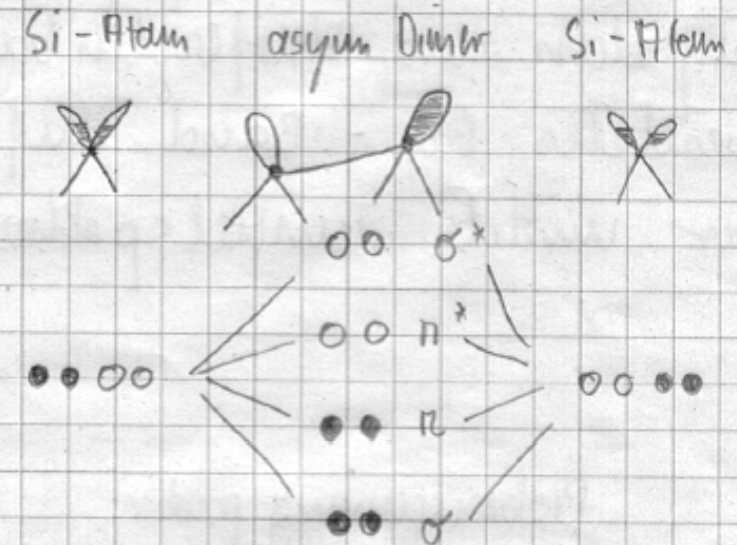
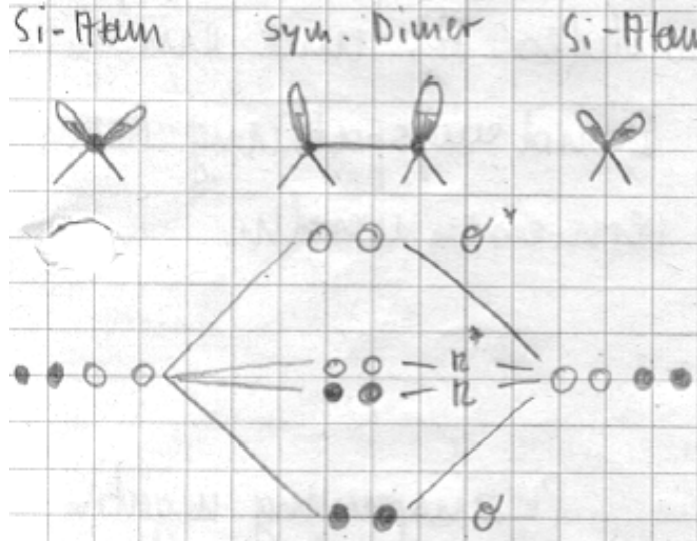


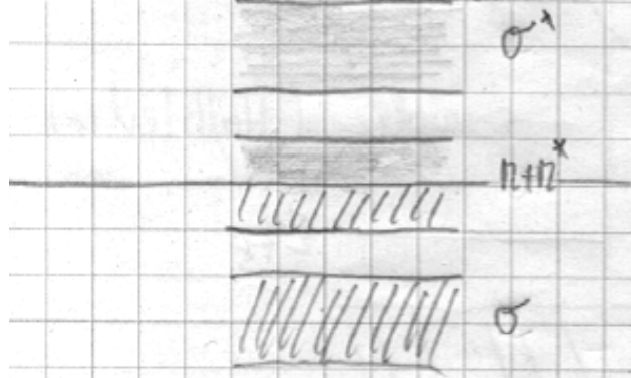
Fig. 1.20

Si(100): Jahn-Teller Type Symmetry Break and Buckled Dimers

Schemta:



Bänderschema:



Aufspaltung

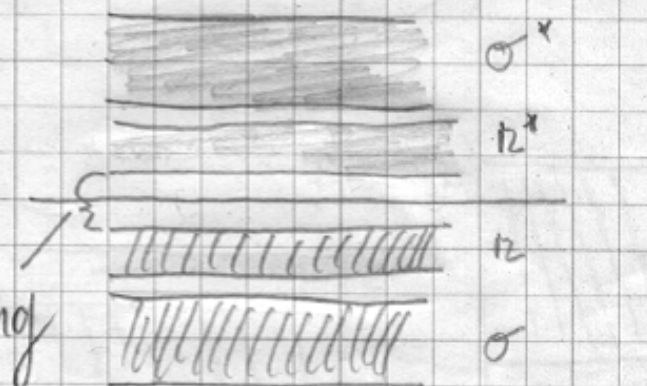
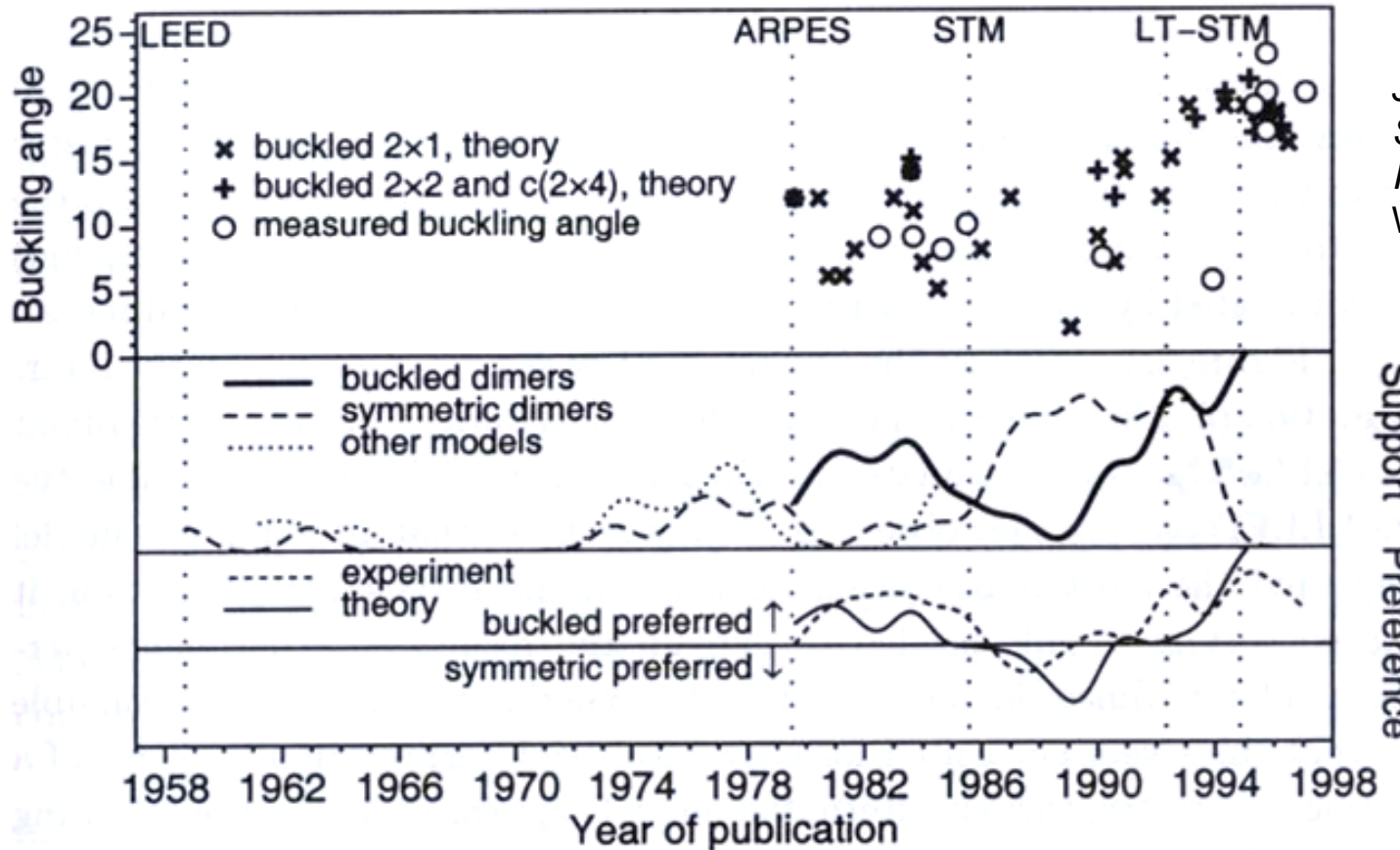


Fig. 1.21

History of Si(100) Reconstruction



J. Darbrowski, H.-J. Müsing,
*Silicon Surfaces and
Formation of Interfaces*
World Scientific 2000, p.85

Fig. 2.1. Development of opinions about the structure of Si(001). Experiments which had a particular impact are indicated by dotted vertical lines. The **upper** panel shows a correlation between the values of the buckling angle which were computed and measured between 1979 and 1997. The **middle** panel shows the support for reconstruction models, measured by the number of published papers; each paper is added as a gaussian with half-width of a year. The theoretical and experimental preference (**lower** panel) is measured by the difference between the number of papers supporting either model. The symmetric dimer model dominated in the period between two STM studies: the first observation of mostly symmetric dimers at room temperature³⁶³ (year 1985) and the first observation of mostly buckled dimers at low temperatures³⁷³ (year 1992).

Fig. 1.22